

1 **The double-edged role of FASII regulator FabT in *Streptococcus pyogenes* infection**

2

3 Clara Lambert^{1†}, Caroline Bachmann¹, Marine Gaillard¹, Antoine Hautcoeur¹, Paprapach
4 Wongdontree², Karine Gloux², Thomas Guilbert¹, Celine Méhats¹, Bastien Prost³, Audrey
5 Solgadi³, Sonia Abreu⁴, Muriel Andrieu¹, Claire Poyart^{1,5}, Alexandra Gruss^{2□} and Agnes
6 Fouet^{1□}.

7

8 ¹Université Paris Cité, Institut Cochin, INSERM, U1016, CNRS, UMR8104, Paris, France;

9 ²Micalis Institute, INRAE, AgroParisTech, Université Paris-Saclay, Jouy en Josas, France;

10 ³UMS-IPSIT - Plateforme SAMM, Université Paris Saclay, France;

11 ⁴Lipides: Systèmes Analytiques et Biologiques, Université Paris-Saclay, 91400 Orsay,

12 France.⁵AP-HP Centre–Université Paris Cité, Paris, France.

13

14 □email: agnes.fouet@inserm.fr ; alexandra.gruss@inrae.fr

15

16 † Present address: Molecular Microbiology and Structural Biochemistry, CNRS, Université de
17 Lyon, Lyon, France

18

19 Orcid numbers: A. Fouet, 0000-0001-7715-9157; A. Gruss, 0000-0001-7426-5229; C.
20 Lambert, 0000-0003-2740-1755; T. Guilbert, 0000-0001-5069-0730

21

22 **Abstract**

23 In *Streptococcus pyogenes*, the fatty acid (FA) synthesis pathway FASII is feedback-controlled
24 by the FabT repressor bound to an acyl-Acyl carrier protein. Despite FabT defects being linked
25 to reduced virulence in animal models, spontaneous *fabT* mutants arise *in vivo*. To resolve this
26 paradox, we characterized the conditions and mechanisms that require FabT activity, and those
27 that promote *fabT* mutant emergence. The primary *fabT* mutant defect is energy dissipation:
28 specific nutrients are consumed, but the mutant fails to grow on human tissue, cells, or cell
29 filtrates where nutrients are limited. These features explain the FabT requirement during
30 infection. Conversely, *fabT* mutants exhibited a marked growth advantage over the wild-type
31 in biotopes rich in saturated FAs. *fabT* mutants emerge in this context, where continued FASII
32 activity prevented environmental FA incorporation. An *ex vivo* muscle model demonstrated that
33 wild-type *S. pyogenes* was inhibited, while *fabT* mutant growth was stimulated, but conditional
34 to FASII activity. Our findings elucidate the rationale for emerging *fabT* mutants that improve
35 survival in lipid-rich biotopes, but lead to a genetic impasse for infection.

36

37 **Introduction**

38

39 Bacterial membranes form a mutable permeable barrier that facilitates adaptation to a changing
40 environment. They usually comprise a phospholipid bilayer composed of a polar head and
41 apolar fatty acid (FA) chains. The FA synthesis pathway (FASII), which is widespread among
42 bacteria, synthesizes saturated and/or unsaturated FAs joined to an acyl carrier protein (ACP;
43 forming acyl-ACP) (Supplementary Fig. 1a). Unsaturated FAs are produced *via* a FASII shunt
44 catalyzed by an acyl-ACP-isomerase named FabM in streptococci. While FASII is conserved
45 (with some enzyme variation), its regulators differ among Firmicutes. In streptococcaceae and
46 enterococcaceae, FASII gene expression is controlled by a unique MarR-family feedback-type
47 regulator named FabT encoded in the main FASII locus (Supplementary Fig. 1 b-c). FabT uses
48 acyl-ACP as corepressor [^{1,2}, for review ³]. The affinity of FabT-(acyl-ACP) binding to a
49 specific DNA palindromic sequence increases with the length of the acyl carbon chain and the
50 presence of an unsaturation ⁴. FabT regulons were characterized in various streptococcaceae
51 species and in conditions that affect membrane FA composition, including growth temperature,
52 pH or growth phase ⁵⁻⁹. FabT exerts greater repression of genes encoding elongation steps,
53 mainly the *trans*-2-enoyl-ACP reductase II FabK, and less repression of *fabM*. In *Streptococcus*
54 *pneumoniae* *fabM* expression is not repressed by FabT ⁶. Accordingly, an *S. pneumoniae* strain
55 lacking a functional FabT produced longer and more saturated FAs ⁶. FabT regulons reportedly
56 also comprise non-FASII genes involved in transport, DNA and carbohydrate metabolism,
57 protein, purine and pyrimidine synthesis; however, their identities vary according to reports and
58 the species under study ³. To date, FabT regulons were not analyzed in the presence of
59 exogenous FAs (eFAs), which enhance FabT transcriptional repression ⁴. This missing
60 information is particularly relevant as numerous host infection sites are FA-rich.

61 *Streptococcus pyogenes*, also known as Group A *Streptococcus*, GAS, is a major human
62 pathogen responsible for a large variety of clinical manifestations ranging from superficial
63 infections to life-threatening invasive infections. GAS infections rank among the top ten causes
64 of death due to bacterial infections worldwide ¹⁰. GAS isolates mutated in *fabT* were recovered
65 in non-human primates at the point of intramuscular inoculation, raising the possibility of such
66 populations forming in the human host ⁵. In a murine model, strains harboring *fabT* point
67 mutations display smaller size lesions, no loss of body weight and a lower mortality than their
68 wild-type counterparts ¹¹. In a non-human primate model, a *fabT* deleted strain shows decreased
69 colonization and dissemination capacities compared to the parental strain ⁵. Its survival is also
70 decreased in human blood or in the presence of human polymorphonuclear leukocytes ⁵.

71 These reported properties indicate that the *fabT* mutant variants are poorly adapted for
72 infection, which led us to question the rationale for their emergence. We solve this question
73 here by performing in-depth analyses of the features of WT and a representative *fabT* mutant
74 in different conditions relevant to host infection. We report that the *fabT* mutant is metabolically
75 wasteful, by consuming sugars and amino acids, yet failing to grow, which accounts for its
76 failure to cause infection. Conversely, saturated FA-rich environments impose a counter-
77 selective pressure against WT bacteria expressing active FabT. We show that *fabT* mutant
78 growth is stimulated around lipid-rich muscle sources in a FASII-dependent manner, while WT
79 growth is inhibited. These findings solve the apparent contradiction between the *in vivo*
80 emergence of attenuated *fabT* variants and the need for an active FabT repressor during
81 infection.

82 **Results**

83

84 **WT and *fabT* mutant growth properties**

85 Multiple independent FabT point mutants were harvested from the infection site of nonhuman
86 primates, some of which mapped to His105⁵. We chose the FabT^{H105Y} point mutation as being
87 representative of mutations that arose *in vivo*, which was established in the *emm28* reference
88 strain M28PF1 (respectively mFabT and WT)^{12,13}(Supplementary Fig. 1b-c)¹⁴. A $\Delta fabT$
89 deletion strain was constructed for comparison. mFabT and WT strains grow similarly in
90 laboratory medium (THY), and in THY supplemented with a C18:1 Δ 9 (oleic acid) source,
91 0.1 % Tween 80 (THY-Tween)². Survival of WT and mFabT strains in mid-exponential phase
92 was also comparable, as assessed by live-dead staining (Supplementary Fig. 2a-b). Unlike
93 mFabT, the $\Delta fabT$ mutant grew slowly in both THY and THY-Tween media (Supplementary
94 Fig. 2c-d; also see¹¹). As *fabT* deletions were not reported to arise *in vivo*, we chose to study
95 the mFabT mutant strain as being representative of *in vivo* mutations.

96

97 **FabT^{H105Y} impacts membrane lipid production and species**

98 The GAS mFabT strain produced greater proportions of longer length saturated FA (C18:0)
99 than the WT strain (26.1 % *versus* 6.8 % respectively; Supplementary Table 1), as first reported
100 in *S. pneumoniae*⁶. In THY-Tween, which supplies C18:1 Δ 9, the native FabT in the WT strain
101 represses FASII, and contains 1.7 times more C18:1 Δ 9 than did mFabT. In this condition, the
102 proportion of C18:0 remained higher in mFabT than in the WT (12.4 % and 0.2 % respectively;
103 Supplementary Table 1)².

104 The effects of the FabT mutation on membrane FA composition should also alter
105 phospholipid metabolism. Lipid analyses of WT and mFabT strains cultured in THY and THY-
106 Tween media identified notable differences in membrane lipid features: i, the primary

107 differences between WT and mFabT FA composition were reflected in all identified lipid
108 species (Supplementary Fig. 3, Supplementary Table 2); ii, THY grown mFabT has ~60 %
109 overall lipid yield compared to that of the WT, extracted from equivalent bacterial OD₆₀₀ (N=4);
110 these differences were narrowed to ~5 % in cultures grown in THY-Tween (Fig. 1a-b,
111 Supplementary Table 3). Among the detected lipids, diglucosyldiacylglycerol (DGDG) and
112 cardiolipin (CL) amounts were proportionately lower in mFabT compared to WT in THY
113 medium. In THY Tween, WT levels of both CL and DGDG decreased. iii, CL species in mFabT
114 were 2-fold enriched in deoxidized cardiolipin (deoxy-CL) species compared to CL in the WT
115 strain, regardless of the growth medium (Fig. 1c-e). CL but not deoxy-CL reportedly facilitates
116 oxidative phosphorylation activity by binding protons¹⁵. In conclusion, the greater proportions
117 of saturated and longer FAs in the *fabT* mutant appear to cause a reduced overall membrane
118 lipid content and alterations in lipid distribution and composition as compared to the WT.

119 *fabT* mutants are reportedly more resistant to the cationic cyclic peptide polymyxin B
120^{5,16}. Polymyxin B binds negatively charged lipids such as CL¹⁷. Putting together these reports
121 and the CL changes noted above, we examined polymyxin B resistance of mFabT and WT
122 strains in conditions where CL amounts varied (Fig. 1f). Features that decreased CL pools, *i.e.*,
123 *fabT* mutation or FA availability during WT growth, correlated with greater polymyxin B
124 resistance. These data support the idea that greater polymyxin B resistance in *fabT* mutants is
125 due to lower CL pools, and show that availability of environmental FAs can lead to polymyxin
126 B resistance. They give a rationale for *fabT* mutant emergence upon polymyxin B selection¹⁶.
127 However, they do not explain the *in vivo* emergence of mFabT mutants at an early stage of GAS
128 infection.

129

130 **Effects of *fabT* on virulence factor expression**

131 In FA-free medium, streptococcal *fabT* truncation or point mutants exhibit an increased *fabK*:
132 *fabM* ratio. FabK and FabM compete for the same substrate to respectively synthesize saturated
133 and unsaturated FAs (Supplementary Fig. 1a). Higher *fabK* expression is thus consistent with
134 the higher proportion of saturated FAs in *fabT* mutants ^{2,6}. Differential *fabK* and *fabM*
135 expression also suggests that these genes may not belong to the same transcriptional unit.
136 Organization of the FASII locus was analyzed by RT-PCR (Supplementary Fig. 4). All genes
137 from *fabM* to *accD* were shown to be cotranscribed. However, transcription start sites are also
138 present within this operon (Fig. 2a) ¹⁸. All transcriptional start sites except that of *fabH* are
139 preceded by a FabT consensus DNA binding motif (5'-ANTTTGATTATCAAATT). This
140 transcriptional organization explains the differential regulation of *fabK* and *fabM*.

141 We performed transcriptomic analyses to identify how the *fabT* mutant and
142 accompanying membrane FA changes might impact and explain the virulence defect during
143 host infection. WT and mFabT expression was compared in THY, and in THY-Tween (as
144 C18:1Δ9 source), which activates WT FabT repression (³ for Review; Supplementary Table 4,
145 Fig 2b-e). Several differences, some corresponding to multi-gene operons, distinguished the
146 two strains (Supplementary Table 4). Notably, purine synthesis operon genes (M28_Spy0022
147 to M28_Spy0026) were upregulated in mFabT, suggestive of increased metabolic activity. An
148 operon encoding adhesins (M28_Spy0107 to M28_Spy0111) was also upregulated; however,
149 expression of virulence genes of the Mga regulon, i.e., C5 peptidase ScpA, and other adhesins,
150 M protein, Sof and SfbX, were down-regulated (Supplementary Table 4). Decreased expression
151 of adhesins and other virulence factors such as SLO (*slo*) and NADase (*nga*) could contribute
152 to the reported poor virulence of *fabT* mutants in infection ¹⁹.

153 Addition of C18:1Δ9 activates FabT-mediated repression, which, as reported, turns off
154 FASII gene expression in the WT strain (Fig. 2c, Supplementary Table 4) ⁴. In contrast, FASII
155 genes, and a non-FASII gene within the FabT regulon (M28_Spy1638, encoding a putative

156 fatty acid kinase binding protein; ¹³), remain transcriptionally active in the mFabT mutant,
157 showing that FabT^{H105Y} is defective for repression (Fig. 2e, Supplementary Table 4). This
158 transcriptional analysis confirms that the single FabT^{H105Y} point mutation loses control of FASII
159 and does not act as a repressor when eFAs are available, and leads to deregulation of virulence
160 genes.

161

162 **The WT strain has a fitness advantage over mFabT during growth on human decidua**

163 To understand the role of *fabT* and emergence of *fabT* mutants, we designed *ex vivo* assays to
164 study infection with WT and *fabT* variants. mFabT strain capacity to colonize human tissue *ex*
165 *vivo* was assessed by measuring its growth on human tissue. As *emm28* strains are associated
166 to puerperal fever ^{20,21}, we compared *ex vivo* growth of WT and mFabT on human decidua ²².
167 In control experiments, both strains failed to grow in RPMI, as assessed by growth ratios
168 between cfus after 8 h incubation and the inocula (Supplementary Fig. 2e). In static conditions,
169 growth of mFabT was 63 % lower than that of the WT strain (Fig. 3a). Growth kinetics of
170 WT^{*eryR-igfp*} and mFabT^{*eryR-igfp*} GFP-marked strains were then followed in flow conditions at the
171 tissue surface by time-lapse microscopy (Fig. 3b-c). The surface colonized by the WT strain
172 increased throughout the 4 h growth period (Fig. 3b). In contrast, mFabT strain growth only
173 increased during the first half-hour of image acquisition. The thickness of bacterial
174 microcolonies increased for the WT, but decreased for the mFabT strain (Fig. 3c). Altogether,
175 the WT strain grew with a doubling time of roughly 200 min whereas the mFabT strain did not
176 grow. Thus, in contrast to normal growth in THY medium, the mFabT strain has a major growth
177 defect in the presence of human decidua. These results provide insight into the nature of the
178 colonization defect and virulence attenuation of *fabT* mutant strains ^{5,11}.

179

180 **Impaired mFabT fitness is due to defective adhesion and poor growth on human cells and**
181 **in cell supernatants**

182 Bacterial colonization of host tissue comprises an initial adhesion step, followed by bacterial
183 multiplication²². As GAS has tropism for endometrial and skin tissues, we compared WT and
184 mFabT adhesion capacities on human endometrial cells, and on differentiated (as present in
185 upper skin layers), and undifferentiated skin keratinocytes (Fig. 3d). The mFabT mutant
186 displayed an adhesion defect on endometrial cells as reported² and undifferentiated
187 keratinocytes compared to the WT. In contrast, the strains adhered similarly on differentiated
188 keratinocytes. The adhesion defect, as also suggested by transcriptome analyses
189 (Supplementary Table 4, Fig. 3d), may contribute to the virulence defect observed in the non-
190 human primate animal models⁵.

191 GAS replicates mainly extracellularly during infection of endometrium and skin²³.
192 Growth comparisons of WT and mFabT strains on these biotopes, namely endometrial cells,
193 undifferentiated keratinocytes, and differentiated keratinocytes, showed that the mFabT strain
194 was decreased (90 %, 53 % and 56 % respectively) compared to the WT strain. The FabT^{H105Y}
195 mutation thus leads to impaired growth in the presence of human cells. To determine whether
196 adhesion is required for the growth differences between WT and *fabT* strains, we assayed
197 bacterial growth in uninfected cell supernatant, termed “conditioned supernatant” (Fig. 3f). The
198 mFabT strain displayed a similar growth defect in endometrial, undifferentiated and
199 differentiated keratinocyte conditioned supernatants (72 %, 50 % and 50 % respectively)
200 compared to the WT. This indicates that cell-secreted products differentially affect growth of
201 WT and mFabT strains. Adhesins differentially produced in WT (Supplementary Table 4, Fig.
202 3d) could also contribute to promoting higher bacterial densities during infection.

203 The differences in WT and mFabT growth were visible when grown on endometrial cells
204 or their conditioned supernatants. It is therefore likely that secreted endometrial cell compounds

205 affecting GAS growth are produced independently of infection. Higher bacterial growth
206 densities on differentiated keratinocytes than on conditioned supernatants (compare Fig. 3e and
207 3f) may be due to greater nutrient availability after infection. Altogether, these data implicate
208 both adhesion and growth defects in poor survival of mFabT in cell infection environments.

209 Poor mFabT growth suggests that mFabT makes inefficient use of nutrients secreted by
210 eukaryotic cells and/or is more susceptible than WT to secreted bactericidal molecules. We
211 investigated growth kinetics of WT and mFabT strains in endometrial cell conditioned
212 supernatant in time course experiments (Fig. 3g left). Cfu ratios were similar for both strains at
213 4 h, indicating no difference in the lag time. However, at 8 h, cfu ratios were higher for the WT
214 strain (Fig. 3f-g left). In addition, mFabT mortality was ~1.5-fold greater than WT at 8 h post-
215 inoculation in conditioned supernatant (Fig. 3g right); these differences are accentuated at 16 h
216 and 24 h (Fig. 3g left). We noted that GAS dies rapidly when growth stops, as seen in RPMI
217 (Supplementary Fig. 2e). We conclude that mFabT grows more slowly and dies more rapidly
218 than the WT strain, and suggest that GAS death is triggered by slow growth.

219

220 **Faster metabolic turnover in mFabT generates a growth defect during infection**

221 We investigated a possible metabolic basis for the mFabT growth defect, which could reflect
222 an incapacity to use cell-secreted products for growth, and/or higher mortality (Fig. 3g). We
223 used a metabolomics approach to assess metabolites that are differentially consumed by mFabT
224 compared to the WT strain, as performed on conditioned supernatants. Hexoses and amino
225 acids, Asn, Gly, Ile and Lys were the main metabolites overproduced by uninfected cells
226 (Supplementary Fig. 5, Supplementary Table 5). The mFabT strain consumed more hexoses
227 and amino acids Asn, Ile, Lys, and Ser, as seen at 16 h (Fig. 4, Supplementary Table 5). This
228 overconsumption is not linked to a higher bacterial yield, but rather the opposite. These data
229 give evidence that the mFabT mutant has a greater metabolic consumption at the GAS site of

230 infection. Thus, the mFabT strain wastes energy during growth: it over-uses amino acids and
231 hexoses compared to the WT strain, but without growth benefits. Futile energy loss, and
232 expression changes in the absence of eFAs, can account for the diminished capacity of *fabT*
233 mutants to cause infection.

234

235 **mFabT is defective for eFA incorporation**

236 C18:1 Δ 9 incorporation is reduced in the mFabT strain (Supplementary Table 1). In *S.*
237 *pneumoniae*, a *fabT* mutant reportedly incorporated only traces of C16:1⁶; in an *Enterococcus*
238 *faecalis fabT* deletion mutant, incorporation of unsaturated FAs, and to a lesser extent, saturated
239 FAs, was defective⁴. We evaluated FA incorporation by GAS in medium supplemented with
240 C17:1, which is not synthesized by GAS; incorporation of this FA generates a discrete peak by
241 gas chromatography (Fig. 5a left). The proportion of C17:1 was 52 % in the WT strain, and 17
242 % in mFabT.

243 Continued FASII synthesis in the mFabT mutant might create competition between
244 endogenously synthesized and eFAs for incorporation into membrane phospholipids. To test
245 this, we performed the same experiments in the presence of platensimycin (Fig. 5a right), a
246 FabF inhibitor that blocks FASII synthesis independently of FabT²⁴. WT and mFabT strains
247 grew similarly in the presence of C17:1 and platensimycin (Supplementary Table 6), and C17:1
248 was the major membrane FA in both strains (Fig. 5a). In conclusion, the FabT^{H105Y} mutant is
249 less responsive to environmental FAs than the WT strain. Poor eFA incorporation in mFabT
250 phospholipids is thus due to continued expression of FASII genes.

251

252 ***De novo* emergence of *fabT* mutants in saturated FA environments**

253 We hypothesized that the defect in eFA incorporation could actually confer a growth advantage
254 to the mFabT strain in toxic lipid environments, and thereby point to conditions of *fabT* mutant

255 emergence. Indeed, FA incorporation can negatively affect bacterial integrity, and free FAs are
256 considered part of the first line of host defense against skin infections ²⁵. Notably, increased
257 C18:0 levels in the mFabT mutant compared to WT (²; Supplementary Table 1) led us to
258 examine saturated FAs as potential selective pressure for *fabT* emergence. WT and mFabT
259 growth and eFA incorporation were then compared in the presence of C14:0 and C16:0, both
260 of which are found among host lipids ²⁶. Both FAs inhibited WT growth, and were nonetheless
261 efficiently incorporated in WT membranes; in striking contrast, mFabT failed to incorporate
262 C14:0, and incorporated >2-fold less C16:0, while strain growth was robust (Fig. 5b-c). This
263 growth advantage incited us to consider that spontaneous *fabT* mutants could emerge in the
264 presence of saturated FAs.

265 As proof of concept, we grew the WT strain in THY liquid medium without or with
266 C14:0, and then streaked cultures on solid medium containing C14:0. Single colonies appeared
267 on this medium, and *fabT* genes were sequenced. Mutations in *fabT* were obtained in both
268 selection procedures, and encoded FabT variants FabT^{T65M} and FabT^{G99S} (Supplementary Fig.
269 1b-c). Both variants were also identified in a primate infection study ⁵. These results provide a
270 rationale for emergence of *fabT* mutants, by generating a growth advantage in lipid-containing
271 biotopes as likely present at the infection locus.

272

273 **Evidence that eFA exclusion by mFabT confers a growth advantage in a simulated muscle** 274 **biotope**

275 We hypothesized that *fabT* mutations could provide a transient advantage in lipid-rich biotopes,
276 which would explain their emergence in muscle ⁵. An *ex vivo* model was devised to assess
277 effects of muscle on GAS growth. For this, commercial organic 15 % fat meat, *i.e.*, muscle
278 from cattle, was placed on lawns of WT^{*eryR-igfp*} and mFabT^{*eryR-igfp*}. Remarkably, WT strains

279 developed a weak inhibitory halo surrounding the muscle samples. In strong contrast, the
280 mFabT strain grew directly and vigorously around muscle sources (Fig. 5d).

281 This result is consistent with growth inhibition of WT but not mFabT GAS, notably by
282 saturated eFAs (Fig. 5b). To confirm that vigorous growth of mFabT around muscle relates to
283 its lower incorporation of FAs from muscle lipids, we tested the effects of adding the FASII
284 inhibitor platensimycin to growth medium and plates. All media contained C17:1, which is
285 incorporated and allows mFabT growth in the presence of the FASII inhibitor (Fig. 5a,
286 Supplementary Table 6). As in Fig. 5d, mFabT growth was robust around muscle sources in the
287 absence of FASII inhibitor (Fig. 5e, upper). In contrast, growth was strongly inhibited around
288 the muscle source when platensimycin was present (Fig 5e lower). The marked inhibitory effect
289 of the muscle sample on the *fabT* mutant when FASII is blocked gives strong evidence that
290 incorporation of muscle lipids negatively affects GAS growth. We conclude that continued
291 FASII activity in mFabT mutants reduces eFA incorporation and thus protects bacteria from
292 toxicity of host lipids as present in muscle biotopes.

293

294 **Discussion**

295 Our work establishes the causal origin for *fabT* mutation emergence and provides an
296 explanation for its disappearance during invasion (Fig. 6): GAS is genetically designed to
297 incorporate eFA from lipid-containing environments, and repress FASII. We showed that WT
298 GAS growth is inhibited by saturated FAs in such environments. Counter-selection can lead to
299 emergence and outgrowth of *fabT* mutants, which explains their detection at a non-invasive
300 step of infection⁵. At this step, the *fabT* mutation would confer a transient advantage over non-
301 mutant strains. We first showed the *fabT* growth advantage, and mutant emergence, using C14:0
302 selection. We then demonstrated that the lipid-rich muscle environment promotes *fabT* mutant
303 growth in a FASII-dependent manner, while inhibiting the WT strain. However, the *fabT*

304 mutation has a cost for virulence: it results in higher mortality and a multiplication defect in the
305 presence of human cells, which is confirmed on human decidua tissue. Continued FASII
306 activity in *fabT* mutant strains provokes a state of futile bacterial metabolism where increased
307 metabolite uptake does not lead to improved growth.

308 Our findings indicate that futile FASII synthesis by mFabT is detrimental for GAS
309 virulence. We showed previously that blocking FASII with antibiotic inhibitors, mutation, or
310 deletion did not prevent infection by *Streptococcus agalactiae*, nor by other Firmicute
311 pathogens²⁷⁻²⁹. FASII inhibition and eFA incorporation in phospholipids corresponds to the
312 natural feedback inhibition in response to eFAs^{3,27}. The contrary, *i.e.*, making FASII synthesis
313 constitutive by inhibiting FabT, is detrimental for *in vivo* infection. FabT is thus a promising
314 target for new therapeutics against specific Gram-positive pathogens including GAS, *S.*
315 *agalactiae*, *S. pneumoniae*, and *E. faecalis*.

316

317 **Methods**

318 **Bacterial strains and culture conditions**

319 The strains used in this study are described in Supplementary Table 7. GAS strains were grown
320 under static condition at 37 °C in Todd Hewitt broth supplemented with 0.2 % Yeast Extract
321 (THY) or on THY agar (THYA) plates, or in brain heart infusion (BHI) liquid or agar medium
322 when specified. Medium was supplemented with 0.1 % Tween 80 (THY-Tween; Sigma-
323 Aldrich, Ref. P1754) as indicated, as a source of C18:1 Δ 9. THY was also supplemented with
324 the saturated FAs, C14:0 and C16:0, in the presence of FA-free bovine serum albumin, 1 mg.ml⁻¹
325 ¹ (Sigma-Aldrich, Ref. A6003) Where indicated, the FASII inhibitor platensimycin (Tebubio,
326 France) was added at (1 μ g/ml). For WT^{eryR-igfp} and mFabT^{eryR-igfp} (Supplementary Table 7)
327 strains, medium was supplemented with 5 or 10 μ g.ml⁻¹ of erythromycin as specified. Strains
328 were prepared as follows, unless specified otherwise: overnight cultures were diluted to an
329 OD₆₀₀ = 0.05 and grown in THY to the exponential phase (OD₆₀₀ comprised between 0.4 and
330 0.5). For GFP expression, exponential-phase bacteria were further diluted to OD₆₀₀ = 0.1 in
331 THY supplemented with 10 μ g.ml⁻¹ erythromycin, and 20 ng.ml⁻¹ anhydrotetracycline to induce
332 GFP expression, grown for 90 min at 37 °C, and diluted in RPMI as indicated below. For growth
333 in saturated FAs, WT and mFabT THY precultures were diluted in THY or THY-C14:0 or
334 THY-C16:0 to OD₆₀₀ = 0.05, transferred to 50 mL falcon tubes, and incubated at 37 °C. Growth
335 was determined by OD₆₀₀ readings at designated time points.

336

337 **Strain construction**

338 Primers used for cloning and strain verification are described in Supplementary Table 8. The
339 Δ FabT strain corresponds to a *fabT* deleted mutant. It was obtained by homologous
340 recombination of the plasmid pG1- Δ FabT following a published protocol ^{30,31}. The DNA
341 fragments encompassing *fabT* were cloned in BamHI – EcoRI digested pG1 using the In Fusion

342 cloning kit® (Clontech). This led to the deletion of *fabT* from nucleotides 49 to 389, as
343 confirmed by PCR. The mFabT^{eryR-igfp} strain harboring an integrated inducible *gfp* gene was
344 constructed as described for the WT^{eryR-igfp} strain²². Whole genome sequencing was performed
345 on the mFabT and mFabT^{eryR-igfp} constructed strains, and no surreptitious mutations were found
346 (Bioproject PRJNA926803, accession number SAMN34247893 for mFabT, SAMN34247911
347 for mFabT^{eryR-igfp}).

348

349 **Fatty acid analysis**

350 Strains were grown until OD₆₀₀ = 0.4 - 0.5. Fatty acids were extracted and analyzed as described
351 ^{2,13,27-29}. Briefly, analyses were performed in a split-splitless injection mode on an AutoSystem
352 XL Gas Chromatograph (Perkin-Elmer) equipped with a ZB-Wax capillary column (30 m x
353 0.25 mm x 0.25 mm; Phenomenex, France). Data were recorded and analyzed by TotalChrom
354 Workstation (Perkin-Elmer). FA peaks were detected between 12 and 40 min of elution, and
355 identified by comparing to retention times of purified esterified FA standards (Mixture ME100,
356 Larodan, Sweden). Results are shown as percent of the specific FA compared to total peak areas
357 (TotalChrom Workstation; Perkin Elmer).

358

359 **Lipid analysis**

360 Strains were grown as 200 ml cultures in THY or THY-Tween until OD₆₀₀ = 0.4 - 0.5. Lipid
361 extractions and identifications were performed as described^{28,32-34}. Lipid separation was
362 realized by normal phase HPLC (U3000 ThermoFisher Scientific) using a Inertsil Si 5µm
363 column (150 x 2.1 mm I.D.) from GL Sciences Inc (Tokyo, Japan). Lipids were quantified using
364 a Corona-CAD Ultra and identified by mass-spectrometry negative ionization and MS²/MS³
365 fragmentations (LTQ-Orbitrap Velos Pro). The concentration of each lipid class was
366 determined as described using as standards DGDG, 840524P-5MG; MGDG, 840523P-5MG;

367 CL (heart CA), 840012P-25MG; PG (egg), 841138P-25MG³⁵. Lipid spectra were analyzed on
368 Xcalibur™ software (ThermoFisher Scientific, version 4.2.47). Lipid concentrations are
369 presented as milligrams per OD₆₀₀ = 100 for all samples.

370

371 **Polymyxin B assay**

372 Polymyxin B sensitivity was assayed as described⁵. Bacteria were grown to OD₆₀₀ = 0.4 - 0.5
373 in THY or THY-Tween. Serial dilutions were prepared in PBS, and 2.5 µl of each dilution was
374 inoculated onto THY or THY-Tween plates containing or not 20 µg.ml⁻¹ polymyxin B (Sigma-
375 Aldrich, Ref. 81271). Plates were incubated at 37 °C for approximately 24 h and photographed.
376 Experiments were done in biological triplicates.

377

378 **In silico analysis**

379 Geneious prime Biomatters development, www.geneious.com was used to identify 5'-
380 ANTTTGATTATCAAATT-3', the putative FabT binding sequence, on the M28PF1 genome,
381 accepting up to 2 mismatches.

382

383 **RNA isolation and Illumina RNA-seq sequencing**

384 GAS strains were cultured at 37°C in THY or THY-Tween, and cells were harvested during
385 exponential growth (OD₆₀₀ between 0.4 and 0.5). Independent triplicate cultures were prepared
386 for each condition. For RNA preparation, 2 volumes of RNA protect* (Qiagen) was added to
387 cultures prior centrifugation (10 min 12,000 g) and total RNA was extracted after lysing
388 bacteria by a 30 min 15 mg.ml⁻¹ lysozyme, 300 U.ml⁻¹ mutanolysin treatment at 20°C followed
389 by two cycles of Fast-prep (power 6, 30 s) at 4 °C. RNA extraction (Macherey-Nagel RNA
390 extraction kit; Germany) was done according to supplier instructions. RNA integrity was
391 analyzed using an Agilent Bioanalyzer (Agilent Biotechnologies, Ca., USA). 23S and 16S

392 rRNA were depleted from the samples using the MICROBExpress Bacterial mRNA enrichment
393 kit (Invitrogen, France); depletion was controlled on Agilent Bioanalyzer (Agilent
394 Biotechnologies). Libraries were prepared using an Illumina TS kit. Libraries were sequenced
395 generating 10,000,000 to 20,000,000 75-bp-long reads per sample.

396

397 **RNA-Seq data analysis**

398 The MGAS6180 strain sequence (NCBI), which is nearly identical to M28PF1^{12,20}, was used
399 as a reference sequence to map sequencing reads using the STAR software (2.5.2b)
400 BIOCONDA (Anaconda Inc). RNA-seq data were analyzed using the *hclust* function and a
401 principal component analysis in R 3.5.1 (version 2018-07-02). For differential expression
402 analysis, normalization and statistical analyses were performed using the SARTools package
403 and DESeq2^{36,37} *p*-values were calculated and adjusted for multiple testing using the false
404 discovery rate controlling procedure³⁸. We used UpsetR to visualize set intersections in a
405 matrix layout comprising the mFabT *versus* the WT strain grown in THY and in THY-Tween,
406 and growth in THY-Tween *versus* THY for each strain^{39,40}.

407

408 ***Ex vivo* GAS growth capacity analysis**

409 Human placentas with attached maternal-fetal membranes were collected and processed as
410 described²² with the following modifications. Tissues were obtained after vaginal delivery, and
411 the samples used were from regions located far from the cervix, known as zone of intact
412 morphology⁴¹. Human decidual explants were infected within hours of their reception.

413 *Ex vivo* bacterial growth capacity in the presence of decidua human tissue was done as
414 follows: exponentially growing GFP-expressing bacteria were washed twice in PBS and diluted
415 in RPMI at a final concentration of 10⁴ bacteria per ml. Decidua tissue were washed twice in
416 PBS. One ml of bacteria were then added to tissue, followed by incubation at 37°C + 5 % CO₂.

417 After 8 h, the tissues were shredded using Precellys Evolution (Bertin Technologies) (6 x 20 s
418 at 5500 rpm with a 20 s pause between shaking). Serial dilutions of shredded material were
419 plated on THYA plates. The number of cfus was determined after 24 h of growth at 37 °C and
420 normalized to the inoculum for each experiment.

421 Live bacterial multiplication on human tissue: infection of maternal-fetal explants, image
422 acquisition and treatments were realized as described ²².

423

424 **Study approval**

425 The study of the human maternal-fetal membranes was approved by the local ethics committee
426 (Comité de Protection des Personnes Ile de France III, no. Am5724-1-COL2991, 05/02/2013).

427 All participants provided written informed consent prior to inclusion in the study at the
428 Department of Obstetrics, Port Royal Maternity, Cochin University Hospital, Paris, France.

429

430 **Cell culture**

431 HEC-1-A (ATCC_ HTB-112TM) endometrial epithelial cells were cultured as recommended,
432 in McCoy's 5A medium (Gibco, Ref. 26600080) supplemented with 10 % fetal bovine serum
433 at 37 °C, 5 % of CO₂. HaCaT (Addex-Bio T0020001) keratinocytes were cultivated as
434 recommended, in DMEM high glucose medium (Gibco, Ref. 31966) supplemented with 10 %
435 fetal bovine serum at 37 °C, 5 % of CO₂. HaCaT cells were maintained in the undifferentiated
436 state by cultivation in poor DMEM medium (Gibco, Ref. 21068-028) supplemented with 1X
437 glutaMax (Gibco, Ref. 35050-038), 1X sodium pyruvate (Gibco, Ref. 11360-039), 2 % fetal
438 bovine serum and 8 % chelated fetal bovine serum using Chelex[®] 100 Resin (BioRad, Ref. 142-
439 1253). To differentiate HaCaT cells, 2.8 mM CaCl₂ (Sigma-Aldrich, Ref. 21115) was added to
440 the medium. Cells were differentiated after seven days as previously described and checked by
441 microscopy ⁴².

442

443 **Bacterial adhesion capacity**

444 GAS adhesion capacity was evaluated as described after growing bacteria in THY to an OD₆₀₀
445 of 0.4 to 0.5³⁰. Values were normalized to the inoculum for each experiment.

446

447 **Bacterial growth capacity in the presence of eukaryotic cells or culture supernatants**

448 GAS were cultured in THY to OD₆₀₀ = 0.4 - 0.5. Bacteria were washed twice in PBS and diluted
449 in RPMI medium without glutamine (Gibco, Ref. 32404-014) to infect cell cultures or inoculate
450 filtered cell culture supernatants (conditioned supernatants) at a final concentration of 10³ and
451 10⁴ bacteria per ml, respectively. Confluent cells in 24-well plates were starved 24 h before the
452 experiment, *i.e.* incubated in RPMI medium without glutamine, and washed twice in PBS. Cells
453 were infected with 1 ml of bacteria and incubated at 37 °C + 5 % CO₂. After 8 h, supernatants
454 were recovered and cells were lysed with 1 ml distilled water. The fractions were pooled and
455 serial dilutions plated on THYA plates. Conditioned supernatants were prepared by incubating
456 cells in 1 ml RPMI at 37°C + 5 % CO₂ for 8 h. The conditioned supernatant was recovered,
457 inoculated with 10³ bacteria, and incubated for another 4, 8, 16 or 24 h. Serial dilutions were
458 plated on THYA plates. The number of cfus was determined after 24 h of growth at 37 °C and
459 normalized to the inoculum for each experiment.

460

461 **Live / dead analysis**

462 After bacterial growth in the HEC-1-A conditioned supernatant during 8 h, bacterial Bacterial
463 mortality was determined using the LIVE/DEAD® BacLight™ Bacterial Viability Kit
464 (ThermoFischer Scientific, Ref. L7012) as described for flow cytometry utilization using an
465 ACCURI C6 cytometer (BD Biosciences, Le pont de Claix, France) from the CYBIO Core

466 Facility. Bacteria were grown in HEC-1-A conditioned supernatant for 8 h for testing. Results
467 of three independent experiments were analyzed using the BD Accuri C6 software.

468

469 **Metabolomic analysis**

470 HEC-1-A conditioned supernatants were inoculated or not with WT or mFabT strains during 8
471 or 16 h and prepared as described above (see ‘Bacterial growth capacity in the presence of
472 eukaryotic cells or culture supernatants’). The metabolite composition of these supernatants
473 was analyzed by Proteigene (<https://proteigene.com>) using MxP® Quant 500 kit (Biocrates) by
474 two analytical methods, LC-MS/MS for small molecules and FIA-MS/MS for lipids. This
475 analysis was repeated on 3 independent series of supernatants and on RPMI. These analyses
476 have a defined detection threshold (LOD) for each family of metabolite.

477

478 **Spontaneous *fabT* mutant isolation**

479 WT strain overnight precultures were diluted either in THY or in THY-C14:0 supplemented
480 with BSA 0.025 %. When the THY culture reached mid-exponential phase, ($OD_{600} = 0.4 - 0.5$),
481 both cultures were streaked on THYA supplemented with C14:0 (THYA-C14:0). Plates were
482 incubated 60 h at 37°C. Colonies were isolated on THYA-C14:0, and isolated colonies were
483 subsequently grown on THYA. Six and eight clones originating from the THY and the THY-
484 C14:0 liquid media, respectively, were used for *fabT* sequencing PCR was performed directly
485 on patched colonies. The oligonucleotides used were FabT-222, and FabTavComp,
486 (Supplementary Table 8) binding 221 bp 5’ from the T of the TTG translation start site and 565
487 bp downstream of it, respectively. The *fabT* gene and surrounding sequences were amplified
488 by PCR using the Green Taq DNA Polymerase, GenScript, according to the manufacturer’s
489 instruction, with 30 cycles with a hybridizing temperature of 50°C and an elongation time of 1
490 min. The Sanger sequencing was carried out by Eurofin Genomics

491 (<https://eurofinsgenomics.eu/en/custom-dna-sequencing/portfolio-overview/>) on PCR
492 products.

493

494 ***Ex vivo* assessment of GAS WT and mFabT growth on muscle (meat) lipids**

495 WT^{eryR-igfp} and mFabT^{eryR-igfp} strains (Supplementary Table 7) ²² were grown overnight in BHI
496 (Ery 5), and then diluted to OD₆₀₀ = 0.05 in FA-free bovine serum albumin (referred to as BSA;
497 0.025%) plus C17:1 100 μM in 1 ml, without or with platensimycin 1 μg/ml, with Ery 5 for
498 selection. After 4 h growth, culture densities were adjusted to OD₆₀₀ = 1 in BHI, and 35 μl were
499 spread on 5 cm diameter plates containing 5 ml BHI agar plus BSA 0.025% and C17:1 100 μM,
500 without or with platensimycin 0.5 μg/ml, with Ery 5 for selection. The muscle samples used
501 were from organic cattle meat bought frozen and pre-ground, containing 15% fat (Picard,
502 France). Absence of contaminants was checked by plating without bacteria. Samples were
503 placed directly on the lawns, and plates were incubated 48 h at 37°C, and photographed. N=4
504 for experiments without platensimycin, and N=2 for those with platensimycin.

505

506 **Statistical analysis**

507 Data were analyzed with GraphPad Prism version 9.4.1. The tests used are indicated in figure
508 legends. Statistical significance is indicated by: ns (not significant, p > 0.05); *, p < 0.05; **, p
509 < 0.01; ***, p < 0.001; ****, p < 0.0001.

510

511 **References**

512

- 513 1 Jerga, A. & Rock, C. O. Acyl-Acyl carrier protein regulates transcription of fatty acid
514 biosynthetic genes via the FabT repressor in *Streptococcus pneumoniae*. *J Biol Chem*
515 **284**, 15364-15368, doi:10.1074/jbc.C109.002410 (2009).
- 516 2 Lambert, C. *et al.* Acyl-AcpB, a FabT corepressor in *Streptococcus pyogenes*. *J*
517 *Bacteriol* **205**, e0027423, doi:10.1128/jb.00274-23 (2023).
- 518 3 Lambert, C., Poyart, C., Gruss, A. & Fouet, A. FabT, a Bacterial Transcriptional
519 Repressor That Limits Futile Fatty Acid Biosynthesis. *Microbiol Mol Biol Rev*,
520 e0002922, doi:10.1128/membr.00029-22 (2022).
- 521 4 Zou, Q., Zhu, L. & Cronan, J. E. The *Enterococcus faecalis* FabT transcription factor
522 regulates fatty acid synthesis in response to exogenous fatty acids. *Front Microbiol* **13**,
523 877582, doi:doi: 10.3389/fmicb.2022.877582 (2022).
- 524 5 Eraso, J. M. *et al.* Genomic Landscape of Intrahost Variation in Group A *Streptococcus*:
525 Repeated and Abundant Mutational Inactivation of the *fabT* Gene Encoding a Regulator
526 of Fatty Acid Synthesis. *Infect Immun* **84**, 3268-3281, doi:10.1128/IAI.00608-16
527 (2016).
- 528 6 Lu, Y. J. & Rock, C. O. Transcriptional regulation of fatty acid biosynthesis in
529 *Streptococcus pneumoniae*. *Mol Microbiol* **59**, 551-566, doi:10.1111/j.1365-
530 2958.2005.04951.x (2006).
- 531 7 Eckhardt, T. H., Skotnicka, D., Kok, J. & Kuipers, O. P. Transcriptional regulation of
532 fatty acid biosynthesis in *Lactococcus lactis*. *J Bacteriol* **195**, 1081-1089,
533 doi:10.1128/JB.02043-12 (2013).
- 534 8 Faustoferri, R. C. *et al.* Regulation of fatty acid biosynthesis by the global regulator
535 CcpA and the local regulator FabT in *Streptococcus mutans*. *Mol Oral Microbiol* **30**,
536 128-146, doi:10.1111/omi.12076 (2015).
- 537 9 Zhang, J. *et al.* Inactivation of Transcriptional Regulator FabT Influences Colony Phase
538 Variation of *Streptococcus pneumoniae*. *mBio* **12**, e0130421, doi:10.1128/mBio.01304-
539 21 (2021).
- 540 10 Carapetis, J. R., Steer, A. C., Mulholland, E. K. & Weber, M. The global burden of
541 group A streptococcal diseases. *Lancet Infect Dis* **5**, 685-694, doi:S1473-
542 3099(05)70267-X [pii] 10.1016/S1473-3099(05)70267-X (2005).
- 543 11 Tatsuno, I. *et al.* Relevance of spontaneous *fabT* mutations to a streptococcal toxic
544 shock syndrome to non-streptococcal toxic shock syndrome transition in the novel-type
545 *Streptococcus pyogenes* isolates that lost a salRK. *APMIS* **124**, 414-424,
546 doi:10.1111/apm.12521 (2016).
- 547 12 Longo, M. *et al.* Complete Genome Sequence of *Streptococcus pyogenes emm28*
548 Clinical Isolate M28PF1, Responsible for a Puerperal Fever. *Genome Announc* **3**,
549 doi:10.1128/genomeA.00750-15 (2015).
- 550 13 Lambert, C. *et al.* A *Streptococcus pyogenes* DegV protein regulates the membrane lipid
551 content and limits the formation of extracellular vesicles. *PLoS One* **18**, e0284402,
552 doi:10.1371/journal.pone.0284402 (2023).
- 553 14 Zuo, G. *et al.* Structural insights into repression of the Pneumococcal fatty acid
554 synthesis pathway by repressor FabT and co-repressor acyl-ACP. *FEBS Lett* **593**, 2730-
555 2741, doi:10.1002/1873-3468.13534 (2019).
- 556 15 Haines, T. H. & Dencher, N. A. Cardiolipin: a proton trap for oxidative phosphorylation.
557 *FEBS Lett* **528**, 35-39, doi:10.1016/s0014-5793(02)03292-1 (2002).

- 558 16 Port, G. C., Vega, L. A., Nylander, A. B. & Caparon, M. G. *Streptococcus pyogenes*
559 polymyxin B-resistant mutants display enhanced ExPortal integrity. *J Bacteriol* **196**,
560 2563-2577, doi:10.1128/JB.01596-14 (2014).
- 561 17 Teuber, M. & Miller, I. R. Selective binding of polymyxin B to negatively charged lipid
562 monolayers. *Biochim Biophys Acta* **467**, 280-289, doi:10.1016/0005-2736(77)90305-4
563 (1977).
- 564 18 Rosinski-Chupin, I., Sauvage, E., Fouet, A., Poyart, C. & Glaser, P. Conserved and
565 specific features of *Streptococcus pyogenes* and *Streptococcus agalactiae*
566 transcriptional landscapes. *BMC Genomics* **20**, 236, doi:10.1186/s12864-019-5613-5
567 (2019).
- 568 19 Zhu, L. *et al.* Contribution of Secreted NADase and Streptolysin O to the Pathogenesis
569 of Epidemic Serotype M1 *Streptococcus pyogenes* Infections. *Am J Pathol* **187**, 605-
570 613, doi:10.1016/j.ajpath.2016.11.003 (2017).
- 571 20 Green, N. M. *et al.* Genome sequence of a serotype M28 strain of group A streptococcus:
572 potential new insights into puerperal sepsis and bacterial disease specificity. *J Infect Dis*
573 **192**, 760-770, doi:10.1086/430618 [pii] 10.1086/430618 (2005).
- 574 21 Plainvert, C. *et al.* Invasive group A streptococcal infections in adults, France (2006-
575 2010). *Clin Microbiol Infect* **18**, 702-710, doi:10.1111/j.1469-0691.2011.03624.x
576 (2012).
- 577 22 Weckel, A. *et al.* *Streptococcus pyogenes* infects human endometrium by limiting the
578 innate immune response. *J Clin Invest* **131**, doi:10.1172/JCI130746 (2021).
- 579 23 Pancholi, V. & Caparon, M. in *Streptococcus pyogenes : Basic Biology to Clinical*
580 *Manifestations* (eds J. J. Ferretti, D. L. Stevens, & V. A. Fischetti) (2016).
- 581 24 Wang, J. *et al.* Platensimycin is a selective FabF inhibitor with potent antibiotic
582 properties. *Nature* **441**, 358-361, doi:10.1038/nature04784 (2006).
- 583 25 Thormar, H. & Hilmarsson, H. The role of microbicidal lipids in host defense against
584 pathogens and their potential as therapeutic agents. *Chem Phys Lipids* **150**, 1-11,
585 doi:10.1016/j.chemphyslip.2007.06.220 (2007).
- 586 26 Ni Raghallaigh, S., Bender, K., Lacey, N., Brennan, L. & Powell, F. C. The fatty acid
587 profile of the skin surface lipid layer in papulopustular rosacea. *Br J Dermatol* **166**, 279-
588 287, doi:10.1111/j.1365-2133.2011.10662.x (2012).
- 589 27 Brinster, S. *et al.* Type II fatty acid synthesis is not a suitable antibiotic target for Gram-
590 positive pathogens. *Nature* **458**, 83-86, doi:10.1038/nature07772 (2009).
- 591 28 Kenanian, G. *et al.* Permissive Fatty Acid Incorporation Promotes Staphylococcal
592 Adaptation to FASII Antibiotics in Host Environments. *Cell Rep* **29**, 3974-3982 e3974,
593 doi:10.1016/j.celrep.2019.11.071 (2019).
- 594 29 Hays, C. *et al.* Type II Fatty Acid Synthesis Pathway and Cyclopropane Ring Formation
595 Are Dispensable during *Enterococcus faecalis* Systemic Infection. *J Bacteriol* **203**,
596 e0022121, doi:10.1128/JB.00221-21 (2021).
- 597 30 Weckel, A. *et al.* The N-terminal domain of the R28 protein promotes *emm28* group A
598 *Streptococcus* adhesion to host cells via direct binding to three integrins. *J Biol Chem*
599 **293**, 16006-16018, doi:10.1074/jbc.RA118.004134 (2018).
- 600 31 Six, A. *et al.* Srr2, a multifaceted adhesin expressed by ST-17 hypervirulent Group B
601 *Streptococcus* involved in binding to both fibrinogen and plasminogen. *Mol Microbiol*
602 **97**, 1209-1222, doi:10.1111/mmi.13097 (2015).
- 603 32 Abreu, S., Solgadi, A. & Chaminade, P. Optimization of normal phase chromatographic
604 conditions for lipid analysis and comparison of associated detection techniques. *J*
605 *Chromatogr A* **1514**, 54-71, doi:10.1016/j.chroma.2017.07.063 (2017).
- 606 33 Bligh, E. G. & Dyer, W. J. A rapid method of total lipid extraction and purification. *Can*
607 *J Biochem Physiol* **37**, 911-917, doi:10.1139/o59-099 (1959).

- 608 34 Thedieck, K. *et al.* The MprF protein is required for lysinylation of phospholipids in
609 listerial membranes and confers resistance to cationic antimicrobial peptides (CAMPs)
610 on *Listeria monocytogenes*. *Mol Microbiol* **62**, 1325-1339, doi:10.1111/j.1365-
611 2958.2006.05452.x (2006).
- 612 35 Moulin, M. *et al.* Sex-specific cardiac cardiolipin remodelling after doxorubicin
613 treatment. *Biol Sex Differ* **6**, 20, doi:10.1186/s13293-015-0039-5 (2015).
- 614 36 Anders, S. *et al.* Count-based differential expression analysis of RNA sequencing data
615 using R and Bioconductor. *Nat Protoc* **8**, 1765-1786, doi:10.1038/nprot.2013.099
616 nprot.2013.099 [pii] (2013).
- 617 37 Varet, H., Brillet-Gueguen, L., Coppee, J. Y. & Dillies, M. A. SARTools: A DESeq2-
618 and EdgeR-Based R Pipeline for Comprehensive Differential Analysis of RNA-Seq
619 Data. *PLoS One* **11**, e0157022, doi:10.1371/journal.pone.0157022 (2016).
- 620 38 Benjamini, Y. & Hochberg, Y. Controlling the False Discovery Rate: A Practical and
621 Powerful Approach to Multiple Testing. *J Royal Statistical Society Series B* **57**, 289-
622 300, doi:10.1111/j.2517-6161.1995.tb02031.x (1995).
- 623 39 Lex, A., Gehlenborg, N., Strobel, H., Vuillemot, R. & Pfister, H. UpSet: Visualization
624 of Intersecting Sets. *IEEE Trans Vis Comput Graph* **20**, 1983-1992,
625 doi:10.1109/TVCG.2014.2346248 (2014).
- 626 40 Conway, J. R., Lex, A. & Gehlenborg, N. UpSetR: an R package for the visualization
627 of intersecting sets and their properties. *Bioinformatics* **33**, 2938-2940,
628 doi:10.1093/bioinformatics/btx364 (2017).
- 629 41 Marcellin, L. *et al.* Immune Modifications in Fetal Membranes Overlying the Cervix
630 Precede Parturition in Humans. *J Immunol* **198**, 1345-1356,
631 doi:10.4049/jimmunol.1601482 (2017).
- 632 42 Malerba, M. *et al.* Epidermal hepcidin is required for neutrophil response to bacterial
633 infection. *J Clin Invest* **130**, 329-334, doi:10.1172/JCI126645 (2020).

634 **Acknowledgments**

635 Expert assistance of Benjamin Saint-Pierre (Genom'IC facility of the Institut Cochin) with
636 transcriptomic experiments is gratefully acknowledged. We thank Alice d'Orfani, Lauryn
637 Moali, Iman Nasr and Laure Detheve, undergraduates in the laboratory for technical help, the
638 Imag'IC and Cybio core facilities of the Institut Cochin, and Cédric Broussard, Virginie Salnot
639 and François Guillonnet for helpful discussions. Jamila Anba-Mondoloni (Micalis Institute)
640 provided valuable comments and suggestions on this work. We also thank the personnel of the
641 CIC Mère-Enfant Cochin-Necker for the human decidua. We acknowledge the use of Alphafold
642 and ChimeraX for FabT *in silico* design, and BioRender for computer-generated models.

643

644 **Funding**

645 CL was supported by Université Paris Cité (BioSPC, n°51809666), FRM (FDT202106012831)
646 and FEMS (FEMS Congress Attendance Grant for poster n° 7875 in 2021 and FEMS grant -
647 LISSSD 2022 n° LISS-213065). This work was supported by DIM One Health
648 (RPH17043DJA) (AF), Agence Nationale de la Recherche (StaphEscape project ANR-16-
649 CE15-0013), and the Fondation pour la Recherche Medicale (DBF20161136769) (AG).
650 IMAG'IC core facility is supported by the National Infrastructure France BioImaging (grant
651 ANR-10-INBS-04).

652

653 **Figure legends**

654

655 **Fig. 1 | FA differences in WT and mFabT strains impact lipid content and composition.**
656 **a, b**, HPLC-MS profiles represent the main lipid classes in WT and mFabT grown in indicated
657 media; lipid profiles and quantifications by class. Lipid concentrations correspond to mg
658 extracted from OD₆₀₀=100 culture. MGDG, monoglucosyldiacylglycerol; DGDG,
659 diglucosyldiacylglycerol ; PG, phosphatidylglycerol; CL, cardiolipin (Supplementary Table 3).
660 **c, d, e** CL species in WT and mFabT, showing deoxidized cardiolipin (deoxy-CL) species
661 (indicated by a 'd' preceding the identification name; see Supplementary Table 2); **a-b**, N=4;
662 **c-d**, N=3. **a, b, e**, 2-way ANOVA, Bonferroni post-test, **p<0.01; ***p<0.001. **f**, Polymyxin
663 B sensitivity. WT and mFabT were precultured to OD₆₀₀ = 0.5 in THY or THY-Tween and
664 dilutions were spotted on the same respective solid medium supplemented or not with
665 polymyxin B (PB). Plates are representative of 3 independent experiments. **a-d**, NL,
666 normalization level; WT, white bars; mFabT, green bars.

668 **Fig. 2 | FabT regulon in the presence of eFAs and genetic organization of the GAS FASII**
669 **genes.** **a**-Schematic representation of the GAS FabT regulon, comprising FASII locus and
670 *fakB4* genes. Gene positions with names below are represented. Red asterisks, putative FabT
671 binding sites; bent arrows, transcription start sites; solid arrow, transcript defined by RT-PCRs;
672 dotted arrows, transcripts¹⁸. **b-e**, Volcano plots of differentially expressed genes, compared as
673 indicated. Volcano plots were constructed using GraphPad Prism, by plotting the negative base
674 10 logarithm of the p value on the y axis, and the log of the fold change (base 2) on the x axis.
675 P-values for comparisons of peak intensities were calculated by t-tests. P_{adj}: calculated p-
676 values were adjusted for multiple testing using the false discovery rate controlling procedure
677 (see Methods section). Gene expression was considered modified in a given condition when the
678 absolute value of log₂-Foldchange (FC) was greater than or equal to 1, with an adjusted p-value
679 ≤ 0.05. Data points with low p-values (highly significant) appear at the top of the plot.

680

681 **Figure 3 | The mFabT strain grows poorly on human tissue ex vivo and displays adhesion**
682 **and growth defects in the presence of human cells or in conditioned cell supernatant.** **a**,
683 Comparison of GAS WT and mFabT cfus after 8 h growth in static conditions in the presence
684 of human decidua tissue. **b-c**, Bacterial multiplication at the tissue surface in flow conditions
685 (live imaging); **b, left**, Visualization of WT-GFP and mFabT-GFP multiplication in 2D; **right**,
686 ratios of areas covered by the two strains. **c, left**, 3D-surface heatmap of bacterial layer
687 thickness at 1 and 4 h. The x, y, and z axes are scaled, color code in μm; **right**, ratio over time
688 of thicknesses of WT^{eryR-igfp} and mFabT^{eryR-igfp} strains. **d-g**, Comparison of WT and mFabT
689 strain adhesion and growth capacities in the presence of human cells, or conditioned
690 supernatants. Endometrial cells, undifferentiated keratinocytes, and differentiated
691 keratinocytes, and their respective conditioned supernatants were used as specified. **d**, adhesion
692 ; **e-f**, growth. **g, left**, Bacterial growth kinetics in endometrial conditioned supernatants (cfu.mL-
693 1); **right**, Live/Dead bacteria were assessed after 8 h growth in conditioned
694 supernatants. Growth experiments were started with 10³ bacteria per ml. Determinations were
695 based on N=5 for **a**, N=3 for **b, c, g**, N=9, 7, 7 for **d** (left to right), N=11, 9, 6 for **e** (left to right)
696 and N=8, 7, 9 for **f** (left to right). Analyses were done by T test and Wilcoxon test for **a, d-f** and

697 2-way ANOVA, Bonferroni post-test for **b, c, g**; * $p < 0.05$; ** $p < 0.01$; *** $p < 0.001$;
698 **** $p < 0.0001$. **d-g**: WT, white bars; mFabT, green bars.

699

700 **Fig. 4 | The mFabT strain is more energy-consuming than the WT strain.** Metabolomic
701 analysis of conditioned supernatants and conditioned supernatants inoculated with WT or
702 mFabT after 8 or 16 h incubation. Carbohydrate and amino acid consumption by the mFabT
703 strain (also see Supplementary Table 5). N=3, 2-way ANOVA, Bonferroni post-test; * $p < 0.05$;
704 ** $p < 0.01$; *** $p < 0.005$; p-values just above the $p = 0.05$ threshold are indicated. Strains and
705 growth times are at right.

706

707 **Fig. 5 | The eFA incorporation defect of mFabT confers a selective advantage in saturated**
708 **eFA environments, and in a simulated muscle biotope.** **a**, FA membrane composition of WT
709 and mFabT strains grown in THY-C17:1 (100 μM), containing or not the FASII-inhibitor
710 platensimycin (1 $\mu\text{g}/\text{mL}^{-1}$). Left, FA profiles; right, quantified proportions of major FAs. Both
711 strains grew in the presence of C17:1 regardless of the presence of platensimycin
712 (Supplementary Table 6). **b**, Growth of WT (left), and mFabT (right) in THY supplemented
713 with 100 μM saturated FAs, C14:0 or C16:0. **c**, **Left**, Incorporation of exogenous C14:0 and
714 C16:0 from cultures described in 'b'. **Right**, Percent C14:0 and C16:0 incorporation from
715 growth experiments at left. For these analyses, N=3, 2-way ANOVA, Bonferroni post-test,
716 * $p < 0.05$; ** $p < 0.01$; *** $p < 0.001$. WT (black lines, white bars) and mFabT (green lines and
717 bars). **d-e**, The indicated strains were spread on solid agar. Pellets of organic ground bovine
718 meat (~15 % fat) were used as muscle source, and were placed on the bacterial lawns. Plates
719 were photographed 36 h after incubation at 37°C. Arrowheads indicate zones of inhibition
720 (black) or growth (white) around muscle sources. N=4. **d**, **Upper**, WT^{eryR-igfp} and mFabT^{eryR-igfp}
721 strains were grown in BHI ery5, and plated on the same solid medium. **Lower**, schematic
722 representation of GAS strain growth inhibition and stimulation by muscle. **e**, mFabT^{eryR-igfp} was
723 grown in BHI ery5 medium containing C17:1 as FA source, without or with platensimycin to
724 turn off FASII. Cultures were then plated on respectively the same solid medium. N = 2.

725

726 **Fig. 6 | Model for emergence of *fabT* mutants that are attenuated for virulence.** **a**,
727 **Saturated FAs (SFAs) in a lipid environment favor mFabT emergence.** Toxic FAs may be
728 present in initial GAS contacts with the host. Counter-selection would lead to emergence of
729 FA-insensitive *fabT* mutants, conferring a growth advantage. In a proof of concept, we show
730 that *fabT* mutants are selected in an SFA environment. **b**, **Host cell environment during**
731 **invasion hinders mFabT growth.** Compared to the WT, *fabT* mutant bacteria fail to develop
732 and die more rapidly when exposed to human cells; they are also impaired for adhesion.
733 Continued FASII activity in *fabT* mutants provokes a state of futile bacterial metabolism where
734 metabolite uptake is stimulated, but does not lead to improved growth. Thus, *fabT* mutants in
735 GAS populations may confer a survival advantage at the inoculation site, but do not withstand
736 host cell infection conditions. Mauve and green circles, WT and mFabT cocci; zoom is on
737 phospholipids. Small yellow circles and lines, lipids and eFA hydrolysis products respectively,
738 small red, blue, pink circles, sugars and amino acid residues. Figure was drawn using
739 BioRender (BioRender.com).

740 **Supplementary Figures**

741

742 **Supplementary Fig. 1 | FabT regulator and FASII pathway in GAS.** **a**, The FASII synthesis
743 pathway comprises a first initiation phase for precursor synthesis, followed by the recursive
744 elongation cycle. The final product, acyl-ACP (acyl-Acyl Carrier Protein), supplies FAs for
745 phospholipid synthesis. FabM (orange) leads to unsaturated FAs; FabK products are saturated.
746 Initiation phase and elongation cycle enzymes are represented in green and red, respectively.
747 **b**, FabT sequence; amino acids involved in DNA binding are in red, and those interacting with
748 acyl-ACP are in blue. Arrow indicates the His105Tyr mutation studied in this work. Magenta
749 star highlights amino acids spontaneously mutated *in vivo* and in a saturated-FA environment
750 (this work). **c**, Overall structure of FabT dimer predicted by Alphafold and adapted with
751 ChimeraX (see references 1-2 in Supplementary Methods); one monomer is represented as
752 multicolored (each color designates a separate domain), and the other is beige. Residues Thr64,
753 Gly99 and His105, in magenta, correspond to mutants obtained in this study.

754

755 **Supplementary Fig. 2 | Impact of FabT mutations on GAS growth.** **a-b**, Live/Dead bacteria,
756 tests, using the LIVE/DEAD® BacLight™ Bacterial Viability Kit, performed on WT and
757 mFabT cultures after growth in the indicated media to OD₆₀₀ = 0.4 - 0.5. **c-d**, Growth curves of
758 WT and $\Delta fabT$ strains in the indicated media. **e**, Ratios of OD₆₀₀ of WT or mFabT strains after
759 8 h over respective initial inocula (10³/ml for each) in RPMI medium; ratio below 1 indicates
760 that bacteria die. **a-d** N=3; **e** N=10; differences in **a**, **b**, and **e** were not statistically significant
761 using T-test. WT, white bars; mFabT, green bars.

762

763 **Supplementary Fig. 3 | Phospholipid membrane composition.** Identification of **a**,
764 monoglucosyldiacylglycerol (MGDG), **b**, diglucosyldiacylglycerol (DGDG), **c**,
765 phosphatidylglycerol (PG), **d**, cardiolipin (CL) and **e**, deoxidized cardiolipin (Deoxy-CL).
766 Lipids are presented as the percentage of each class to the total lipids, and are quantified in
767 Supplementary Table 2. Statistical values were determined using 2-way ANOVA, Bonferroni
768 post-test. *p<0.05; **p<0.01; ***p<0.001; ****p<0.0001. Strains were grown in THY (open
769 bars) and THY-Tween (hatched bars). WT, black lines and white bars; mFabT, green lines and
770 bars.

771

772 **Supplementary Fig. 4 | mRNA transcript analysis of FASII locus genes.** Agarose gel of PCR
773 amplification products on cDNA using primer pairs from neighboring genes. MW, molecular
774 weight reference (Generuler 100 bp, ThermoFisher Scientific). Lane 1, *fabM-fabT* (234 bp); 2,
775 *fabH-acpA* (221 bp); 3, *acpA-fabK* (302 bp); 4, *fabZ-accC* (105 bp); 5, *accD-serS* (288 bp).
776 Results confirm the FASII transcriptional units indicated in Fig. 2a.

777

778 **Supplementary Fig. 5 | Carbohydrates and amino acid residues produced by human**
779 **endometrial cells.** Metabolomic analysis of RPMI and HEC-1-A conditioned supernatants, as
780 per legend at right on figure. (see Supplementary Table 5 for complete data). N=3, 2-way
781 ANOVA, Bonferroni post-test; *p<0.05; ***p<0.005; ****p<0.001.

782

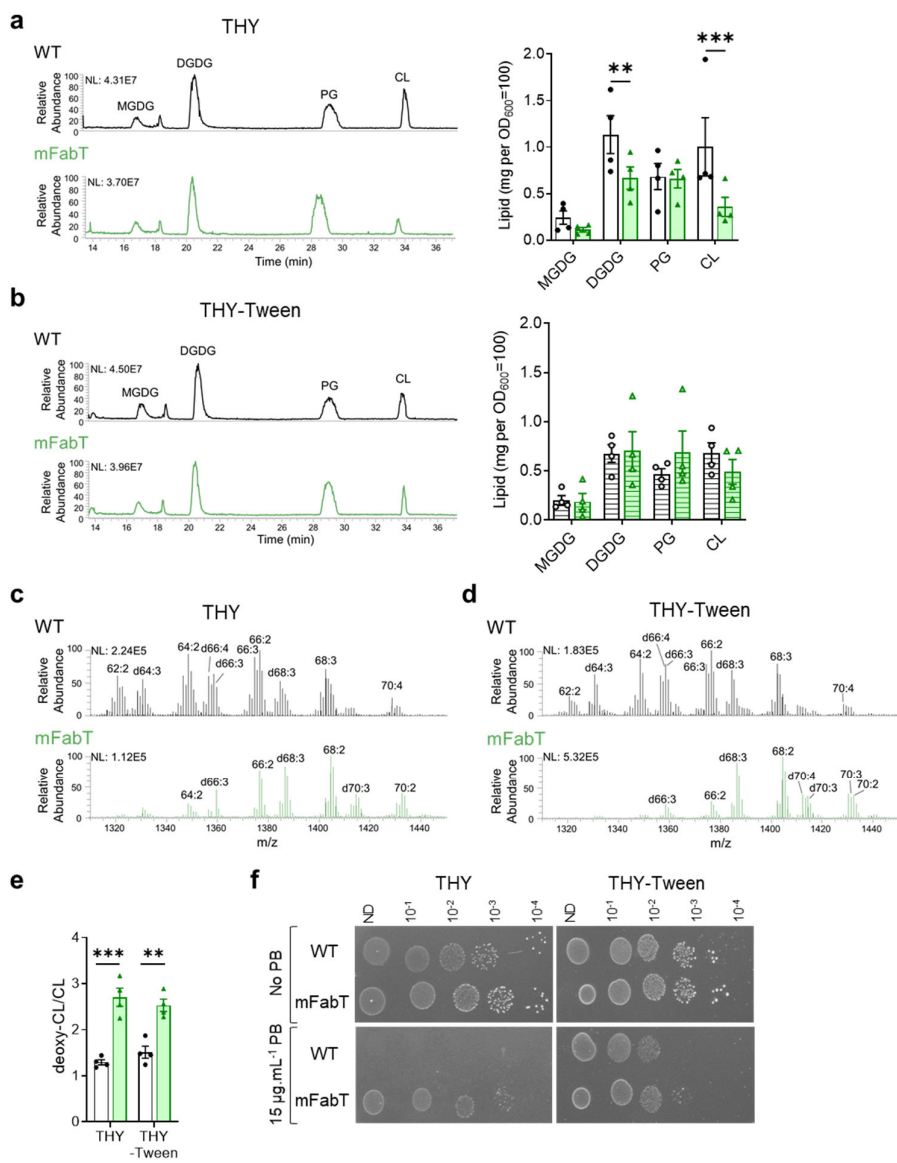
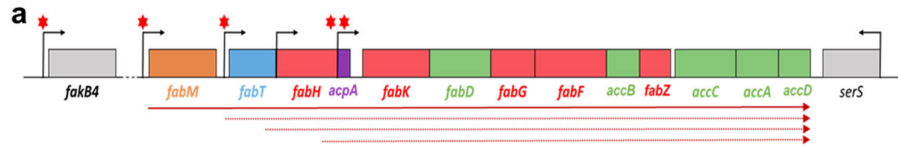
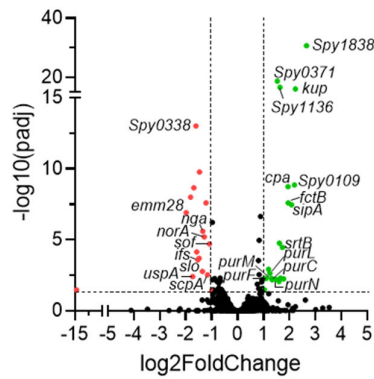


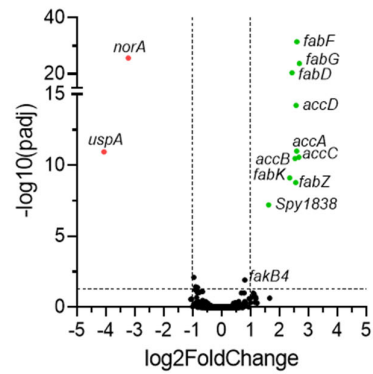
Fig. 1



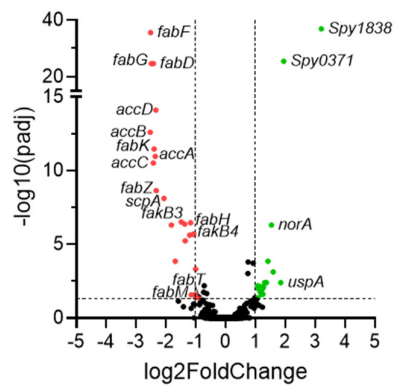
b mFabT vs WT in THY



c mFabT vs WT in THY-Tween



d WT in THY-Tween vs THY



e mFabT in THY-Tween vs THY

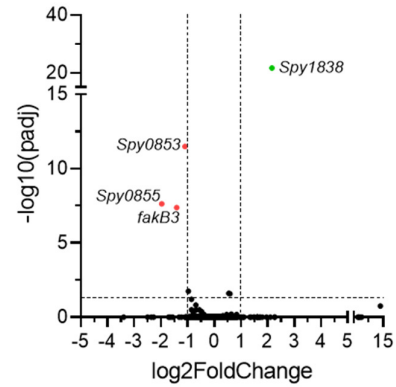


Fig. 2

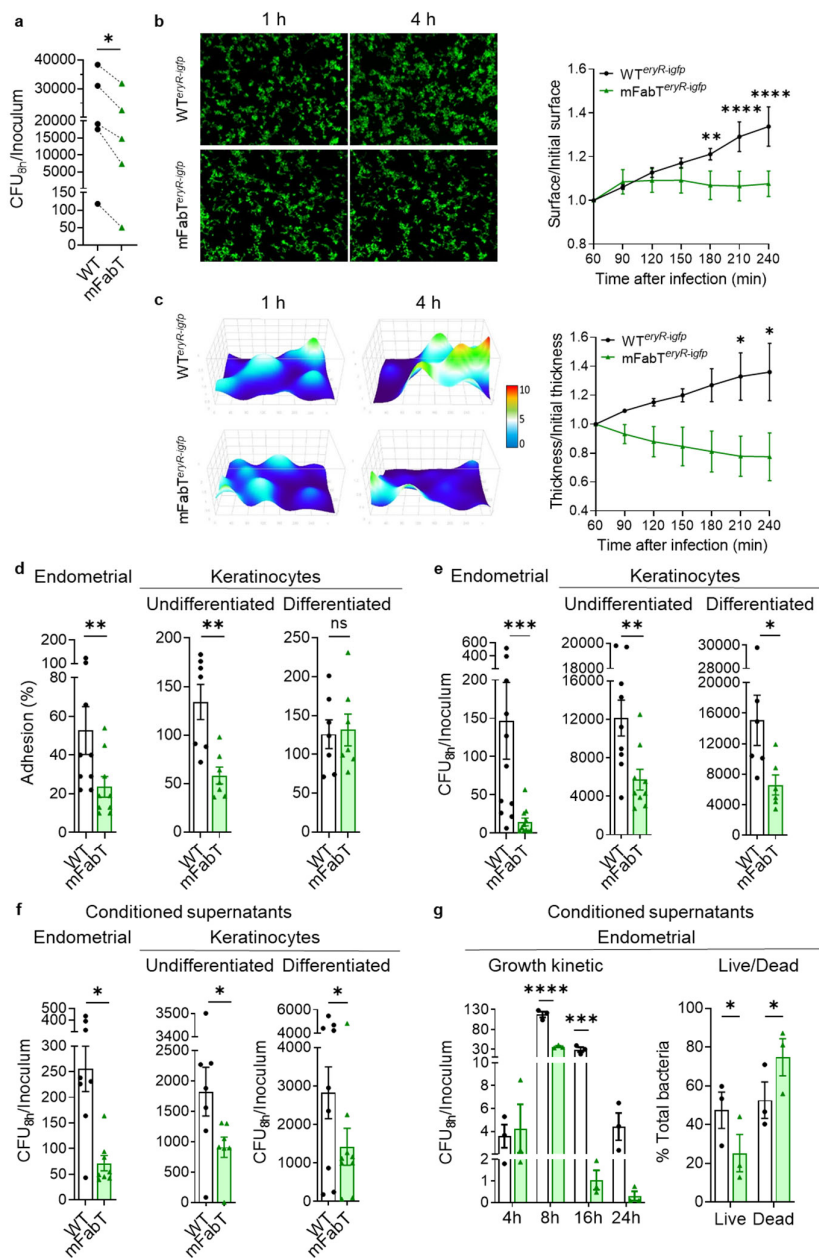


Fig. 3

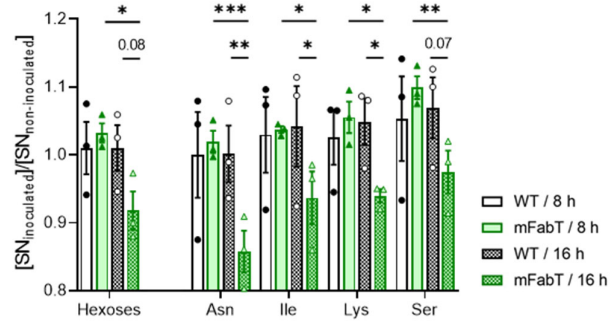


Fig. 4

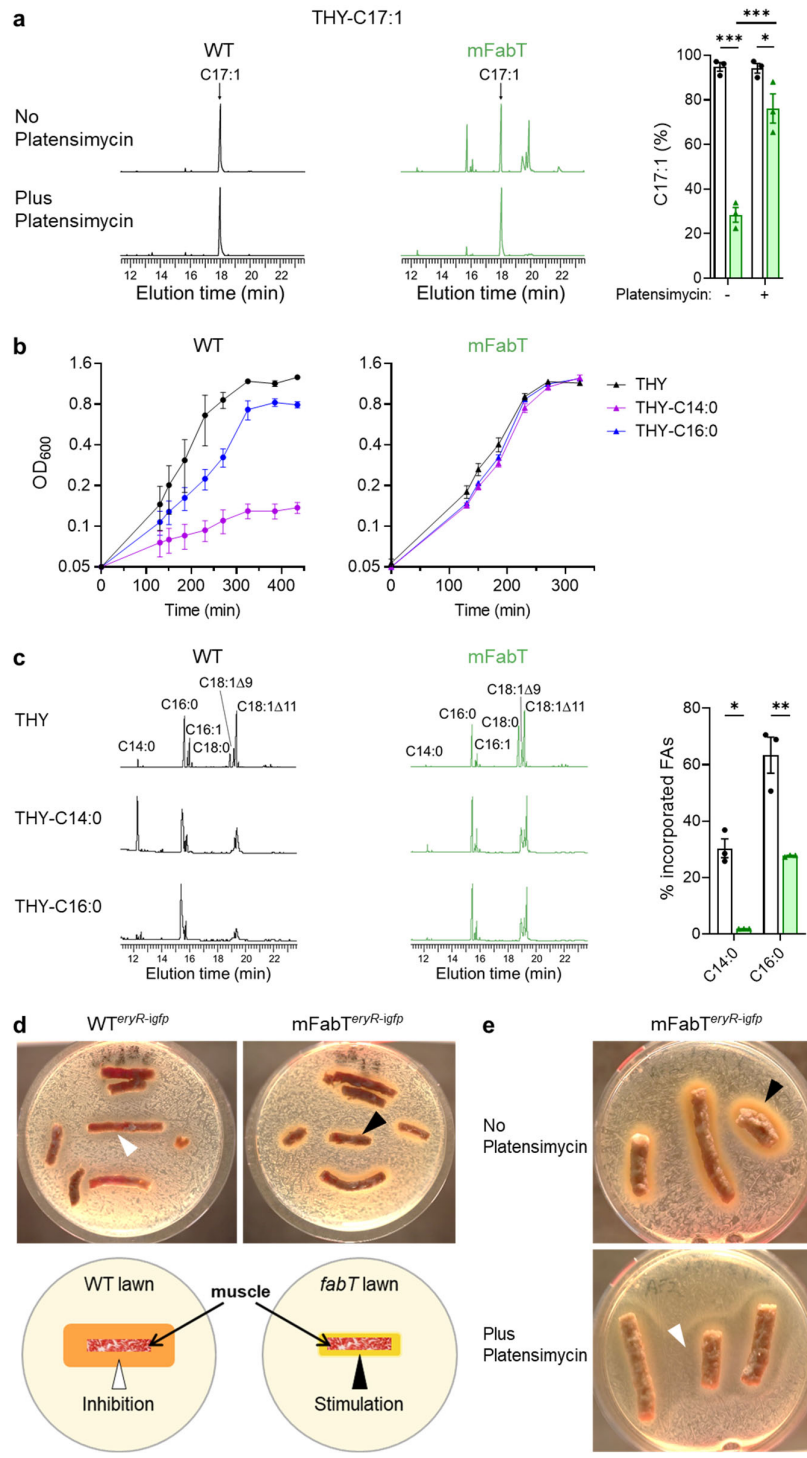


Fig. 5

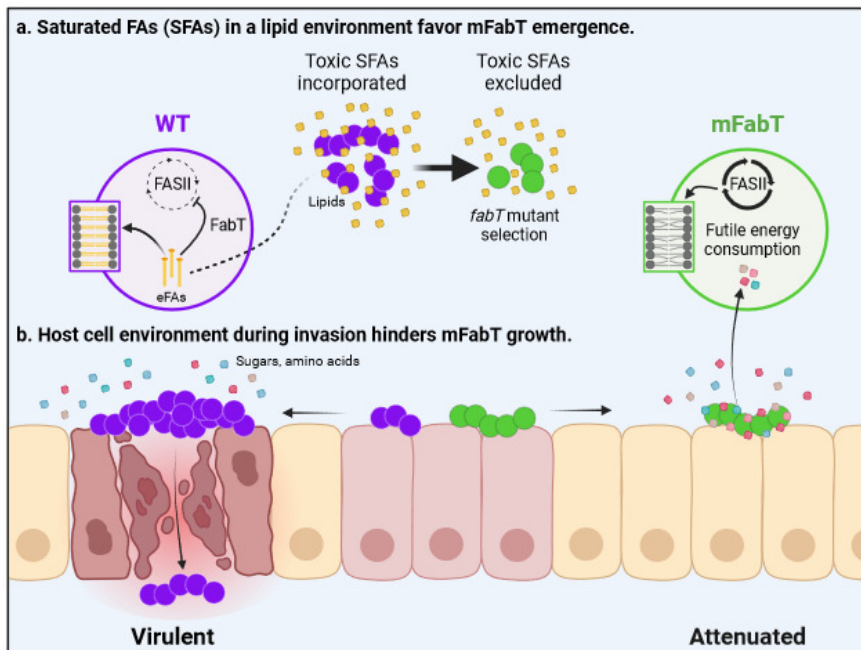
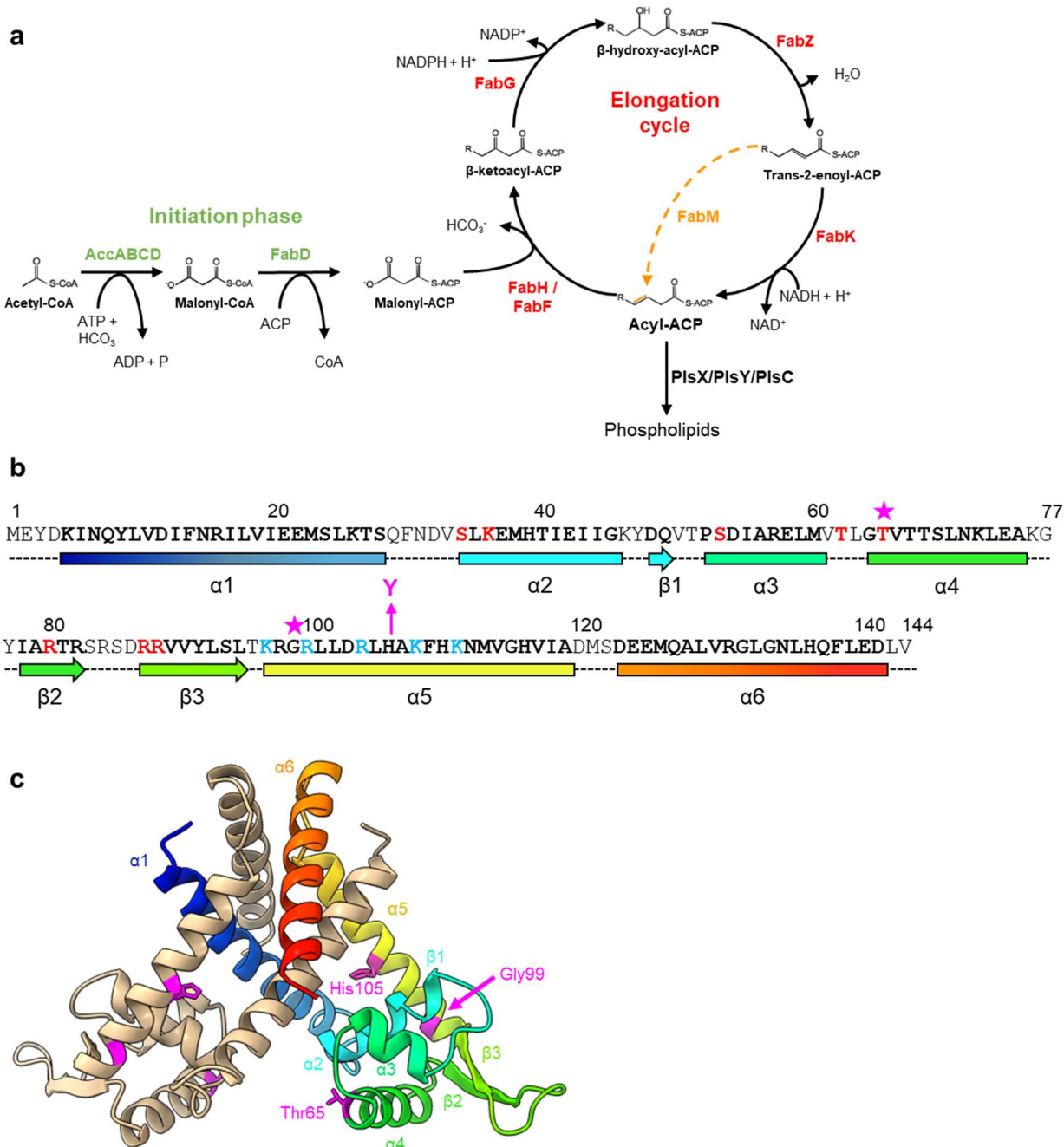
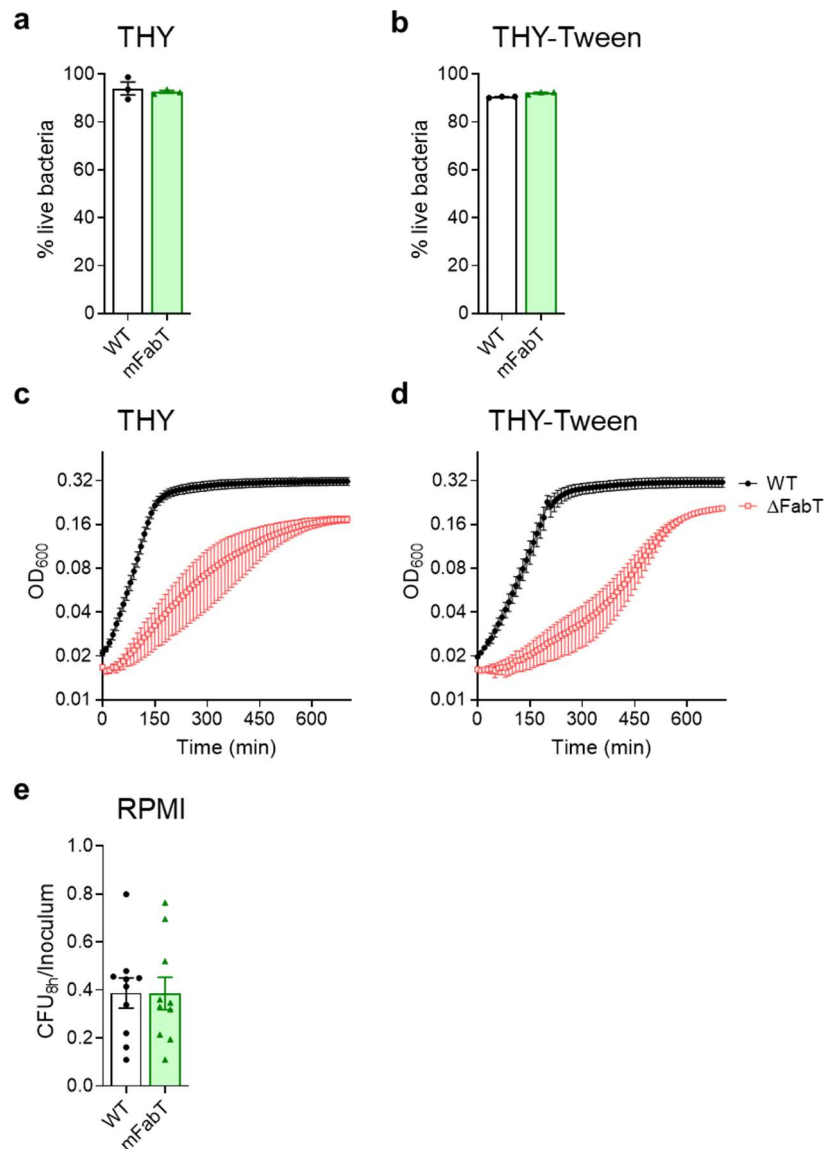


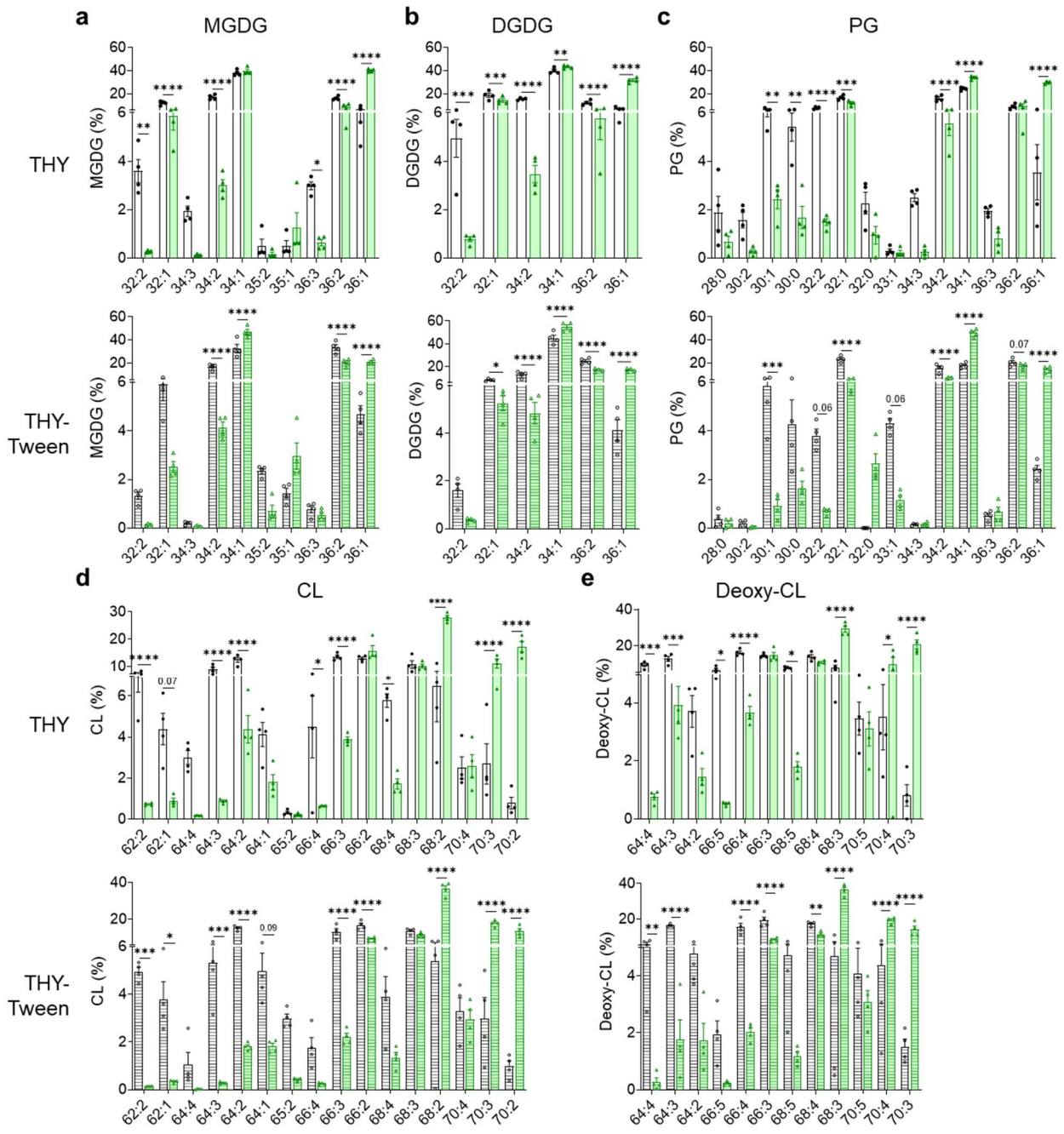
Fig. 6



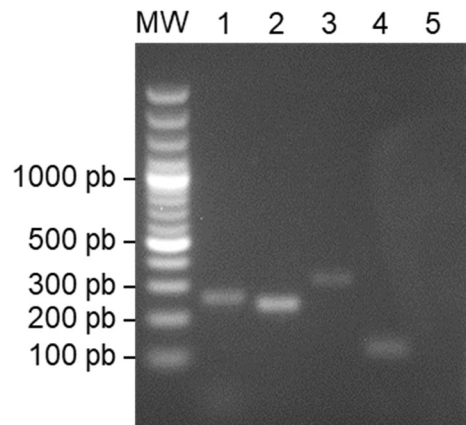
Supplementary Fig. 1 | FabT regulator and FASII pathway in GAS. a, The FASII synthesis pathway comprises a first initiation phase for precursor synthesis, followed by the recursive elongation cycle. The final product, acyl-ACP (acyl-Acyl Carrier Protein), supplies FAs for phospholipid synthesis. FabM (orange) leads to unsaturated FAs; FabK products are saturated. Initiation phase and elongation cycle enzymes are represented in green and red, respectively. **b**, FabT sequence; amino acids involved in DNA binding are in red, and those interacting with acyl-ACP are in blue. Arrow indicates the His105Tyr mutation studied in this work. Magenta star highlights amino acids spontaneously mutated *in vivo* and in a saturated-FA environment (this work). **c**, Overall structure of FabT dimer predicted by Alphafold and adapted with ChimeraX (see references 1-2 in Supplementary Methods); one monomer is represented as multicolored (each color designates a separate domain), and the other is beige. Residues Thr65, Gly99 and His105, in magenta, correspond to mutants obtained in this study.



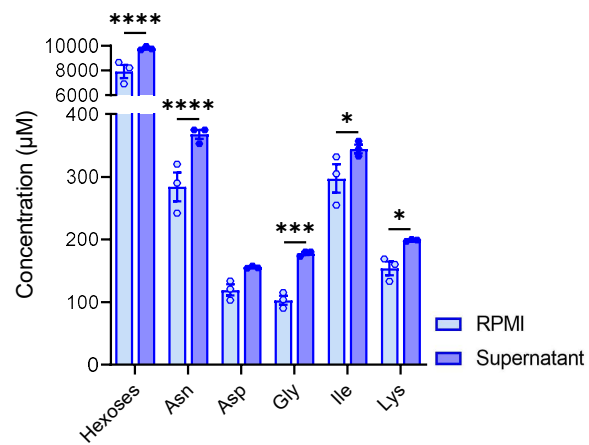
Supplementary Fig. 2 | Impact of FabT mutations on GAS growth. **a-b**, Live/Dead bacteria, tests, using the LIVE/DEAD® BacLight™ Bacterial Viability Kit, performed on WT and mFabT cultures after growth in the indicated media to OD₆₀₀ = 0.4 - 0.5. **c-d**, Growth curves of WT and Δ *fabT* strains in the indicated media. **e**, Ratios of OD₆₀₀ of WT or mFabT strains after 8 h over respective initial inocula (10³/ml for each) in RPMI medium; ratio below 1 indicates that bacteria die. **a-d** N=3; **e** N=10; differences in **a**, **b**, and **e** were not statistically significant using T-test. WT, white bars; mFabT, green bars.



Supplementary Fig. 3 | Phospholipid membrane composition. Identification of **a**, monoglucosyldiacylglycerol (MGDG), **b**, diglucosyldiacylglycerol (DGDG), **c**, phosphatidylglycerol (PG), **d**, cardiolipin (CL) and **e**, deoxidized cardiolipin (Deoxy-CL). Lipids are presented as the percentage of each class to the total lipids, and are quantified in Supplementary Table 2. Statistical values were determined using 2-way ANOVA, Bonferroni post-test. * $p < 0.05$; ** $p < 0.01$; *** $p < 0.001$; **** $p < 0.0001$. Strains were grown in THY (open bars) and THY-Tween (hatched bars). WT, black lines and white bars; mFabT, green lines and bars.



Supplementary Fig. 4 | mRNA transcript analysis of FASII locus genes. Agarose gel of PCR amplification products on cDNA using primer pairs from neighboring genes. MW, molecular weight reference (Generuler 100 bp, ThermoFisher Scientific). Lane 1, *fabM-fabT* (234 bp); 2, *fabH-acpA* (221 bp); 3, *acpA-fabK* (302 bp); 4, *fabZ-accC* (105 bp); 5, *accD-serS* (288 bp). Results confirm the FASII transcriptional units indicated in Fig. 2a.



Supplementary Fig. 5 | Carbohydrates and amino acid residues produced by the human endometrial cells. Metabolomic analysis of RPMI and HEC-1-A conditioned supernatants, as per legend at right on figure. (see Extended Data Table 4 for complete data). N=3, 2-way ANOVA, Bonferroni post-test; * $p < 0.05$; *** $p < 0.005$; **** $p < 0.001$.

The double-edged role of FASII regulator FabT in *Streptococcus pyogenes* infection

Clara Lambert¹, Caroline Bachmann¹, Marine Gaillard¹, Antoine Hautcoeur¹, Paprapach Wongdontree², Karine Gloux², Thomas Guilbert¹, Celine Méhats¹, Bastien Prost³, Audrey Solgadi³, Sonia Abreu⁴, Muriel Andrieu¹, Claire Poyart^{1,5}, Alexandra Gruss²□ and Agnes Fouet¹□.

Supplementary Methods

FabT modelling. Overall structure of FabT dimer (supplementary Figure 1) was predicted by AlphaFold ¹. We used UCSF ChimeraX ² for molecular graphics and further analyses. ChimeraX was developed by the Resource for Biocomputing, Visualization, and Informatics at the University of California, San Francisco, with support from NIH R01-GM129325 and the Office of Cyber Infrastructure and Computational Biology, NIAID.

Live - dead analysis. Bacterial mortality was determined using the LIVE/DEAD® BacLight™ Bacterial Viability Kit (ThermoFisher Scientific, Ref. L7012) as described for flow cytometry utilization using an ACCURI C6 cytometer (BD Biosciences, Le pont de Claix, France) from the CYBIO Core Facility. Bacteria were grown in HEC-1-A conditioned supernatant for 8 h for testing. Results of three independent experiments were analyzed using the BD Accuri C6 software.

Growth curves. GAS stationary precultures were diluted in THY or THY-Tween to an OD₆₀₀ = 0.05, and transferred to 96-well plates, which were incubated at 37 °C in a Thermo Scientific Multiskan GO (ThermoFischer Scientific). Growth was determined by shaking plates immediately before measuring absorbance at OD₆₀₀ every 10 min.

GAS growth capacity analysis in RPMI. GAS bacteria were grown in THY to an $OD_{600} = 0.4$ to 0.5 . Cultures were washed twice in PBS and diluted in RPMI medium without glutamine (Gibco, Ref. 32404-014) to a final concentration of 10^3 bacteria per ml, and then incubated at $37^\circ\text{C} + 5\% \text{CO}_2$ for 8 h. Serial dilutions were plated on THYA solid medium. Cfus were determined after 24 h growth at 37°C and normalized to the inoculum for each experiment.

Screening for FA sensitivity on solid medium. Overnight WT and mFabT cultures were grown starting from single colonies on solid medium containing 0.5% bovine serum albumin. Cultures were then adjusted to $OD_{600} = 0.1$, and $100\ \mu\text{l}$ was spread as a lawn on plates. Four μl ($0.1\ \mu\text{m}$) of each FA (25 mM stocks) were deposited. Plates were incubated 24 h at 37°C and photographed.

References for supplementary material

In supplementary Methods

- 1 Jumper, J. *et al.* Highly accurate protein structure prediction with AlphaFold. *Nature* **596**, 583-589, doi:10.1038/s41586-021-03819-2 (2021).
- 2 Pettersen, E. F. *et al.* UCSF ChimeraX: Structure visualization for researchers, educators, and developers. *Protein Sci* **30**, 70-82, doi:10.1002/pro.3943 (2021).